# Table of Contents (TOC)

**Continuous Wafer-Scale Graphene on cubic-SiC(001)**

Alexander N. Chaika[1,2,*], Olga V. Molodtsova[3], Alexei A. Zakharov[4], Dmitry Marchenko[5], Jaime Sánchez-Barriga[5], Andrei Varykhalov[5], Igor V. Shvets[2], Victor Yu. Aristov[1,3]

[1]Institute of Solid State Physics RAS, Chernogolovka, Moscow District 142432, Russia
[2]Centre for Research on Adaptive Nanostructures and Nanodevices (CRANN), School of Physics, Trinity College, Dublin 2, Ireland
[3]HASYLAB at DESY, D-22607 Hamburg, Germany
[4]MAX-lab, Lund University, Box 118, 22100 Lund, Sweden
[5]Helmholtz-Zentrum Berlin für Materialien und Energie, D-12489 Berlin, Germany

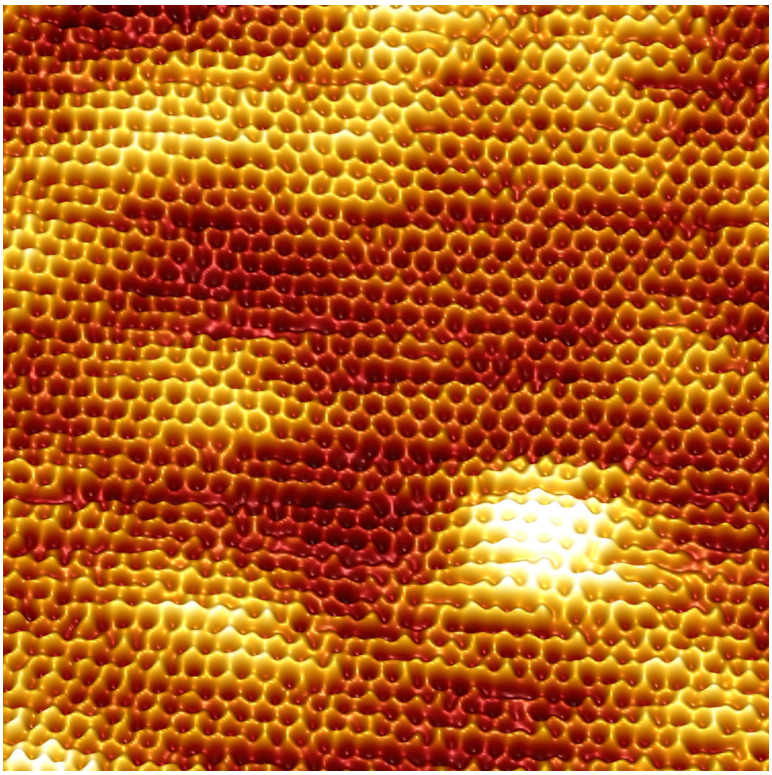

Low energy electron microscopy, scanning tunneling microscopy, and angle resolved photoelectron spectroscopy studies prove the millimeter-scale continuity and uniform thickness of the graphene synthesized on cubic-SiC(001)/Si(001) wafers. The graphene overlayer on SiC(001) consists of only a few non-interacting monolayers with the atomic and electronic structure of freestanding, single-layer graphene.

Nano Res
DOI (automatically inserted by the publisher)
Research Article **Please choose one**

# Continuous Wafer-Scale Graphene on cubic-SiC(001)

Alexander N. Chaika[1,2](✉), Olga V. Molodtsova[3], Alexei A. Zakharov[4], Dmitry Marchenko[5], Jaime Sánchez-Barriga[5], Andrei Varykhalov[5], Igor V. Shvets[2], Victor Yu. Aristov[1,3]

[1]Institute of Solid State Physics RAS, Chernogolovka, Moscow District 142432, Russia

[2]Centre for Research on Adaptive Nanostructures and Nanodevices (CRANN), School of Physics, Trinity College, Dublin 2, Ireland

[3]HASYLAB at DESY, D-22607 Hamburg, Germany

[4]MAX-lab, Lund University, Box 118, 22100 Lund, Sweden

[5]Helmholtz-Zentrum Berlin für Materialien und Energie, D-12489 Berlin, Germany

Received: day month year / Revised: day month year / Accepted: day month year (automatically inserted by the publisher)


## ABSTRACT

The atomic and electronic structure of graphene synthesized on commercially available cubic-SiC(001)/Si(001) wafers have been studied by low energy electron microscopy (LEEM), scanning tunneling microscopy (STM), low energy electron diffraction (LEED), and angle resolved photoelectron spectroscopy (ARPES). LEEM and STM data prove the wafer-scale continuity and uniform thickness of the graphene overlayer on SiC(001). LEEM, STM and ARPES studies reveal that the graphene overlayer on SiC(001) consists of only a few non-interacting monolayers with the physical properties of freestanding, single-layer graphene. Atomically resolved STM and micro-LEED data show that the top graphene layer consists of nanometer-sized domains with four different lattice orientations connected through the <110>-directed boundaries. ARPES studies reveal the typical electron spectrum of graphene with the Dirac points close to the Fermi level. Thus, the use of cheap SiC(001)/Si(001) wafers for graphene fabrication represents a realistic way of bridging the gap between the outstanding properties of graphene and their technological applications.

## KEYWORDS

Graphene, Cubic-SiC(001), STM, ARPES, LEEM, LEED

Unique electronic properties [1-3] make graphene an appealing candidate for novel non-silicon-based electronics. Graphene synthesis on the surface of alpha silicon-carbide (α-SiC) under vacuum [4,5] or argon atmosphere at high pressure [6] is the best method developed so far for graphene fabrication on isolating substrates. Nevertheless, this method does not meet the requirements of industrial mass production because of the limited size and high costs of bulk α-SiC wafers. The growth of graphene on cubic-SiC films deposited on Si wafers has also been studied in recent years [7-12]. However, most studies have been carried out on the (111) surfaces which can not be easily

Address correspondence to chaika@issp.ac.ru (Alexander N. Chaika)

adapted for nanoelectronic technologies. If graphene layers could be fabricated on the surface of thin SiC films grown on low cost large-diameter Si(001) wafers (SiC virtual substrates), the industrial impact would be enormous. In particular, graphene synthesized on commercially available cubic-SiC(001)/Si(001) wafers could be easily adapted for graphene-based electronic technologies and directly patterned using industrial Si lithographic processes. Silicon carbide substrates are also highly promising for graphene synthesis because several monolayers of graphene on SiC reveal the same physical properties as a freestanding graphene monolayer [3,13]. This can facilitate graphene/SiC treatments and open new perspectives for future applications.

The first reports of graphene growth on the surface of cubic-SiC(001) thin films (with thickness of about 1 μm) deposited on a Si wafer have been published recently [11,12]. However, the existing experimental data cannot provide unambiguous information on the atomic and electronic structure of the graphene layers on the SiC(001) surface, their continuity and the uniformity of their thickness on a wafer scale which are crucial for potential applications. In this work we prove the feasibility of continuous graphene overlayer synthesis on SiC(001)/Si(001) wafers compatible with existing electronic technologies. The results of comprehensive low energy electron microscopy (LEEM), scanning tunneling microscopy (STM), angle-resolved photoelectron spectroscopy (ARPES) and low energy electron diffraction (LEED) studies demonstrate reproducible synthesis of graphene coverage consisting of few non-interacting monolayers on millimeter-scale areas of SiC(001). LEEM and STM studies prove the wafer-scale continuity and uniform thickness of the graphene overlayer. Atomically resolved STM and ARPES studies show that the synthesized graphene layers interact weakly with the SiC substrate and therefore possess the intrinsic properties of a freestanding graphene monolayer as proved earlier for graphene synthesized on $\alpha$-SiC [3,13].

Uniform graphene layers were fabricated on SiC(001)/Si(001) wafers using Si-atom sublimation followed by SiC surface layer graphitization during high-temperature annealing in the ultrahigh vacuum (UHV) STM chamber. With increasing annealing temperature from 800°C to 1300°C, Si-rich 3×2 and 5×2, Si-terminated stoichiometric c(4×2) and C-terminated stoichiometric SiC(001)-c(2×2) reconstructions [14-18] were successively formed, as confirmed by our LEED and atomically resolved STM data. To convert the carbon–carbon bonds of the c(2×2) surface structure into $sp^2$ graphene bonds, flash heating at elevated temperatures (1300–1350°C) was applied. Only short flashes not exceeding 30 seconds were used for graphene fabrication to minimize Si atom desorption at elevated temperatures and the growth of multilayer graphite-like structures [9,19,20]. The base pressure in the STM chamber was in the range of 4-6×$10^{-11}$ mbar. It did not exceed 2×$10^{-10}$ mbar during the high-temperature flashing of well-outgassed samples and rapidly recovered after graphene synthesis. This allowed the preparation of continuous and uniform millimeter-scale graphene layers free of contaminants. The synthesized graphene on SiC(001) was first studied in-situ by atomically resolved STM. Before LEEM and ARPES measurements, the graphene/SiC(001) samples were annealed at temperatures of 200-1000°C to remove contaminants which could appear during transfer from the STM chamber to the corresponding endstations. The conclusions on the continuity of the graphene overlayer on SiC(001), and its atomic and electronic structure are based on LEEM, LEED, STM, and ARPES data obtained from several samples and numerous spatially separated surface regions. The qualitative agreement of the results obtained from several samples prove the uniform graphene coverage throughout the millimeter-scale SiC(001)/Si(001) surfaces. In this paper, we show

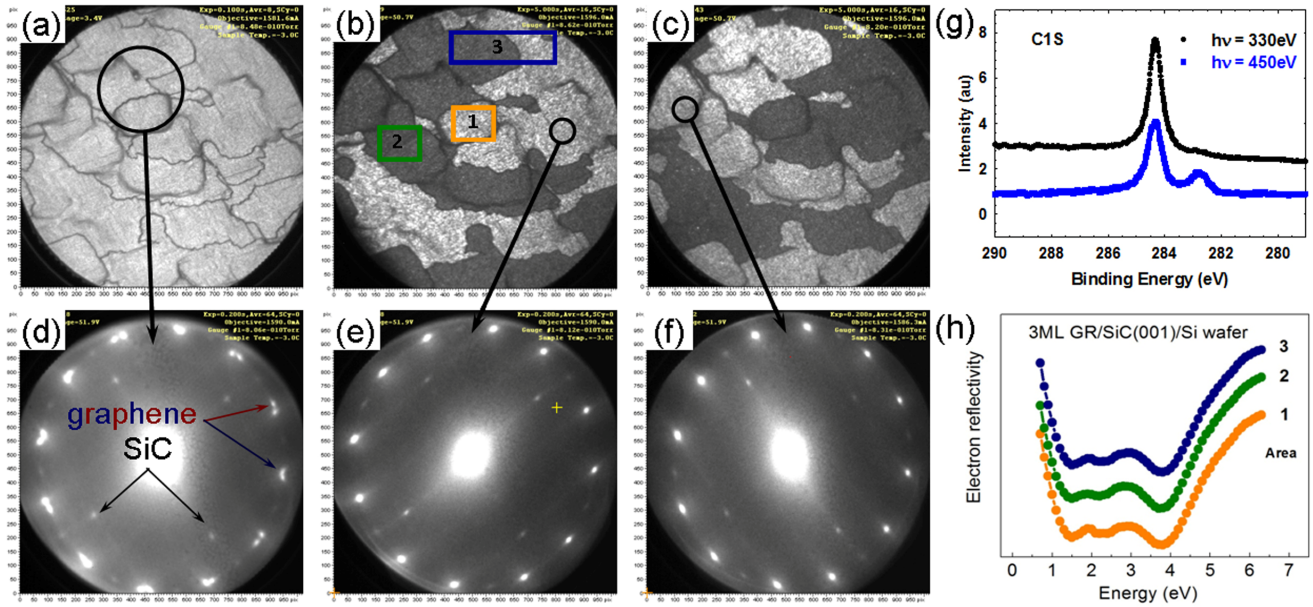


**Figure 1.** (a) 20μm LEEM micrograph, recorded with an electron energy of 3.4 eV, proving the uniform thickness of the graphene synthesized on SiC(001)/Si(001) wafers. (b,c) DF LEEM images from different diffraction spots (shown in panels (e) and (f)) demonstrating the contrast reversal on micrometer scale graphene areas with two rotated domain families. (d-f) Micro-LEED patterns from the surface areas shown in panels (a-c). The sampling areas are 5 μm (a) and 1.5 μm (b,c), E=52 eV. (g) Micro-PES C 1s core level spectra taken from the same sample at different photon energies. The sampling area is 10 μm. (h) Electron reflectivity spectra recorded for the different surface regions 1, 2 and 3 as labelled in panel (b), where the number of dips in the spectra identifies regions 1-3 as trilayer graphene [21,22].

this for trilayer graphene synthesized on SiC(001).

Fig. 1a shows a typical LEEM micrograph (E=3.4 eV) of the graphene/SiC(001) surface demonstrating intrinsic SiC grain boundaries and uniform contrast throughout the probed 20 μm surface area. The uniform contrast in Fig. 1a proves that despite all the defects of the starting cubic-SiC substrate, the thickness of the synthesized graphene is uniform across the probed surface area [6]. The number of graphene layers can be deduced from the reflectivity curves acquired in a 7eV energy window [21,22]. As Fig.1h illustrates, there are three distinct minima in the reflectivity which correspond to the three layers of graphene. The graphene coverage is very homogeneous all over the surface and IV curves are almost identical at different locations on the surface, including areas with different contrast in Dark-Field (DF) LEEM images (*e.g.*, areas 1-3 in Fig.1b).

The micro-LEED pattern taken from a 5 μm area reveals 12 double-split diffraction spots from the graphene layer and well resolved spots from the SiC(001) substrate (Fig. 1d). DF LEEM images of the same surface area (Fig. 1b and 1c) and micro-LEED patterns taken from different 1.5 μm areas, shown in Fig. 1e and 1f, demonstrate that the 12 double-split spots originate from different micrometer-scale surface areas producing 90°-rotated micro-LEED patterns with 12 non-equidistant spots (Fig. 1e and 1f). These areas appear as white and dark in corresponding reflexes (Fig. 1b and 1c). The intensity of the substrate spots at the LEED energy used (52eV) implies that the overlayer thickness does not exceed 3 monolayers of graphene. This conclusion was confirmed by core level C1s photoemission spectra taken from the same

samples. As an example, two spectra measured at different photon energies are shown in Fig. 1g. The C1s spectra reveal only two narrow components with binding energies corresponding to the SiC substrate (lower energies) and graphene layer (higher energies) that proves the absence of a buffer layer and the weak interaction of the synthesized graphene with the SiC substrate. The relative intensities of the components at two photon energies show that the graphene thickness is about three monolayers, which is in accordance with the IV reflectivity data. STM and ARPES studies also prove the freestanding character of the graphene layers on SiC(001) and disclose the origin of the 12 double-split diffraction spots in the micro-LEED patterns (Fig. 1d). As speculated by Ouerghi et al. [12], this splitting could be ascribed either to misorientation of two layers in bilayer graphene or to the presence of four different domains in the single layer. The explanation based on the bilayer of graphene is implausible as one would have to assume that the two layers are rotated with respect to each other by a certain angle that is maintained the same throughout the entire sample and remarkably, is the same for all the samples studied. Our detailed STM and ARPES studies showed that rotated domains within the single graphene layer are responsible for the 24 diffraction spots in the LEED patterns.

Large area STM images show that the top graphene layer on SiC(001) consists of domains with lateral dimensions ranging from several nm to 20–30 nm connected through the grain boundaries. The domains are typically elongated along one of the <110> directions of the SiC crystal lattice (Fig. 2a) and possess a rippled morphology, which leads to a root mean square roughness of the micrometer-scale STM images ranging from 2.5 to 3.0 Å. These values are typical of a freestanding graphene monolayer [23,24], which can exhibit bumps with heights up to several nanometers [23]. The bumps observed in our studies do not indicate

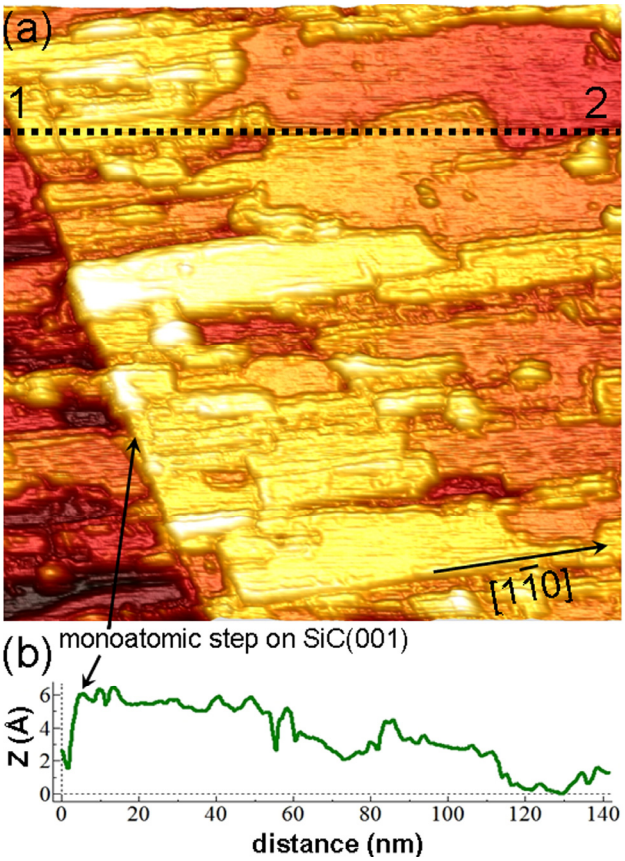


**Figure 2.** (a) A 143 nm × 143 nm STM image of the graphene layer on SiC(001) measured at U = -0.8 V and I = 60 pA. (b) Cross-section 1-2 of the image in panel (a). The height of the monoatomic step, indicated by the arrow in the cross-section, is consistent with the SiC lattice parameter.

either a roughness of the SiC substrate under the graphene layer or the presence of impurities on the surface. According to our STM data (not presented here) the root mean square roughness of the SiC(001)-c(2×2) surface prior to graphene synthesis was below 1.5 Å. Furthermore, our distance-dependent atomically resolved STM studies (Fig. S2) clearly show that the apparent roughness of the graphene layer on SiC(001) can be easily modified by decreasing the tunneling gap (increasing tip-sample interaction). This is related to the high flexibility of the graphene layer weakly interacting with lower lying atomic layers similar to that observed in STM experiments on $SiO_2$ [25]. The

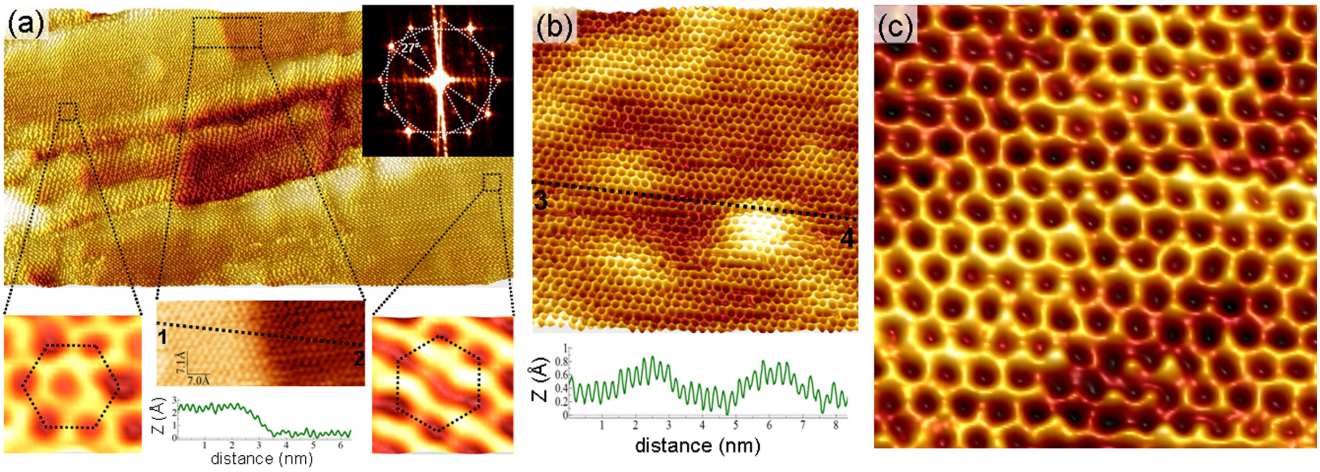


**Figure 3.** (a-c) Atomically resolved STM images of graphene on a cubic-SiC(001) surface. The images were measured at U = 10 mV and I = 60 pA (a), U = 22 mV and I = 70 pA (b), and U = 10 mV and I = 150 pA (c). Inset in Part a (top panel) shows the FFT of the image obtained with WSXM software [26]. The bottom panels of Part a show zooms of the regions indicated by dashed black rectangles and the cross-section 1-2 of the image. The rotated hexagons are indicated on the left and right windows of the bottom panel for clarity. The bottom panel of Part b shows the profile 3-4 indicated in the top panel image of the rippled graphene.

flexibility and rippling of the graphene layer on SiC(001) prove the weak interaction of the graphene layers in fabricated trilayer graphene/SiC(001).

The bumps in large-area STM images are also not related to the presence of multilayer graphite-like domains with different thicknesses, because we measured the same reflectivity spectra with three distinct minima in different spatially separated surface regions in LEEM experiments (Fig. 1h) and did not resolve any mono- or multiatomic steps typical of multilayer graphite in atomically resolved STM studies. The monoatomic step typical of the silicon carbide substrate under the graphene overlayer is clearly visible in Fig. 2a, proving that the applied graphene fabrication procedure does not produce thick multilayer graphite-like structures which would hide all the information about the morphology of the starting SiC(001) surface. The integrity of the graphene coverage and the absence of uncovered SiC(001) regions are proved by the tunneling parameters used for stable large area imaging. The bias voltages in all STM studies of the graphene/SiC(001) system were below 1 V, *i.e.* within the band gap of the SiC (2.3 eV). It is known that stable imaging of the Si- and C-rich SiC(001) surface reconstructions [14-18] is not generally possible at such small voltages. Thus, a coexistence of a graphene overlayer and bare SiC(001) regions can be ruled out from the STM data.

Fig. 3a shows an atomically resolved STM image of the graphene region containing three nanometer-sized domains. The domain images reveal the characteristic periodicity of the graphene lattice and rippling [24]. Zooms of the STM image taken from two different surface regions (bottom panel of Fig. 3a) demonstrate that the graphene lattices in the two domains are rotated by approximately 30°. For precise measurements of the misorientation we removed the thermal drift and scanner axes' non-orthogonalities using the periodicity of the graphene lattice which was overlaid onto the bottom part of the STM image in Fig. 3a (lower lying domain). Under the assumption of constant drift, undesirable distortions of the lattices should be the same for the top and bottom graphene domains. The Fast Fourier Transform (FFT) of the corrected STM image (shown as inset in

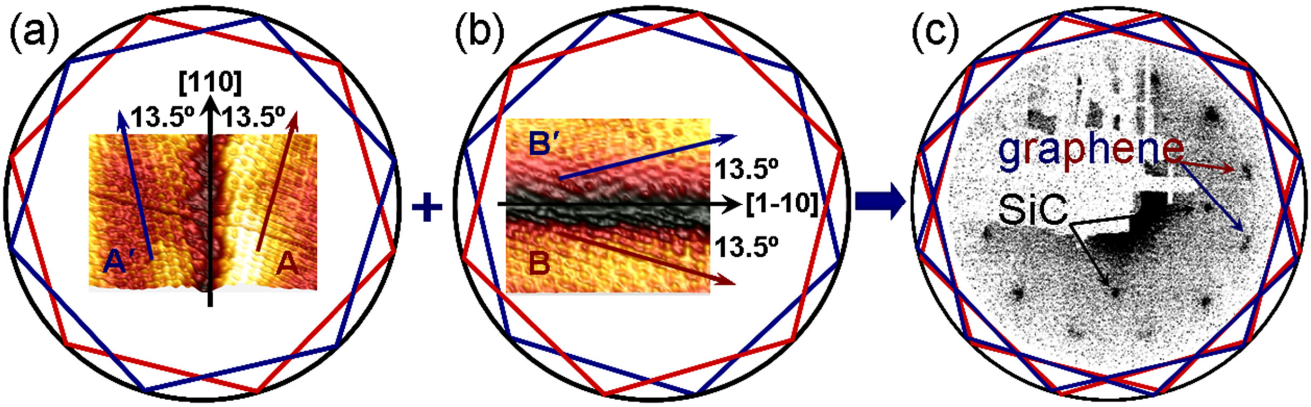


**Figure 4.** (a-c) The model explaining the origin of 24 diffraction spots and Dirac points in LEED and ARPES data. Insets in panels (a) and (b) are STM data confirming the model used. Inset in (c) shows a typical LEED pattern taken from graphene/SiC(001) samples at $E_p$=65 eV demonstrating 1×1 substrate spots along with 12 double-split graphene monolayer spots.

Fig. 3a) reveals two systems of spots (indicated by hexagons) rotated by 27°. It can be noted that this misorientation angle between different domains was found in the electron microscopy studies of a suspended polycrystalline graphene membrane [27]. Such misorientation of domain lattices must be responsible for the 12 non-equidistant diffraction spots seen in the FFT of the atomically resolved STM image (inset in Fig. 3a) and micro-LEED patterns taken from small surface regions (Fig. 1e and 1f). Atomically resolved STM studies revealed that graphene domains were typically elongated in one of the two equivalent <110> directions and appeared in images as nanoribbons with grain boundaries along either [110] or [1-10] direction of the substrate. Figures 2a and 3a show only one of the two possible systems of the domains with the 27°-rotated graphene lattices, but both systems (with horizontal and vertical nanoribbons) were observed in our STM experiments. The atomic resolution images of the two families of domains with graphene lattices rotated by ±13.5° from the [110] and [1-10] directions produced FFT patterns with 12 non-equidistant spots. According to our STM data, these two families, producing four types of domains, are responsible for the 24 diffraction spots as schematically shown in Fig. 4. The two domains rotated by ±13.5° from the [110] axis produce two hexagons of spots (red and blue in Fig. 4a) rotated by 27° with respect to each other. Likewise, the two domains rotated by ±13.5° from the [1-10] axis produce another 12 spots marked again by blue and red hexagons in Fig. 4b. As the hexagons of the [110] family are rotated with respect to the ones of the [1-10] family by 90°, the blue (red) marked hexagon of one family is rotated by 117° with respect to the red (blue) marked hexagon of another family, meaning they nearly superimpose on each other, producing the impression of the double split LEED reflexes (Figs. 1d and 4c).

DF LEEM images in Fig. 1b and 1c distinguish the surface areas containing different domain families. The μ-LEED patterns, recorded from ~1.5 μm surface areas shown in Fig. 1e and 1f, contain 12 non-equally spaced spots, similar to the FFT pattern of the high resolution STM image shown in Fig. 3a. If a large surface area is probed by LEED one can see the superposition of the two diffraction patterns rotated by 90° (Figs. 1d and 4c) in accordance with the model shown in Fig. 4. The DF LEEM images from either A or B reflexes of the well resolved 24-spot-pattern show a reversed contrast and confirm that the 27°-rotated domain regions have a

typical size of several microns (Fig. 1b and 1c). The appearance of two rotated domain families on SiC(001) can be related to intrinsic defects of the cubic-SiC crystal lattice (Fig. 1a-c). However, these defects do not break the continuity and uniform thickness of the graphene coverage, as the LEEM image in Fig. 1a and the reflectivity data in Fig. 1h prove.

Atomic resolution STM studies reveal the rippled morphology within the surface layer domains (Fig. 3b). As illustrated by the cross section in Fig. 3b, the lateral and vertical dimensions of the ripples are about 30–50 Å and 1 Å, respectively, which coincide with the theoretically predicted values for a freestanding graphene monolayer [23]. The cross section and zoom of the top domain in Fig. 3a also demonstrate that there is no periodicity breaking in the domain region appearing in the STM image as an atomic step. This proves that the observed roughness of the top graphene layer is only related to intrinsic rippling because of the weak interaction with the underlying atomic layers. Apparently, the graphene layer is attached to the SiC surface only in those places where graphene boundaries are observed. At the same time, other domain regions rather weakly interact with the substrate and can exhibit the atomic and electronic structure of freestanding graphene.

Apart from the typical 2D layer rippling, STM images reveal the theoretically predicted [24] asymmetric distortion of the carbon-carbon bond lengths (Fig. 3c) and additional electron density modulations near the ribbon edges (*e.g.*, the elevated regions in Fig. 2a and the white regions near the boundary between two 27°-rotated graphene domains in the bottom right corner of Fig.

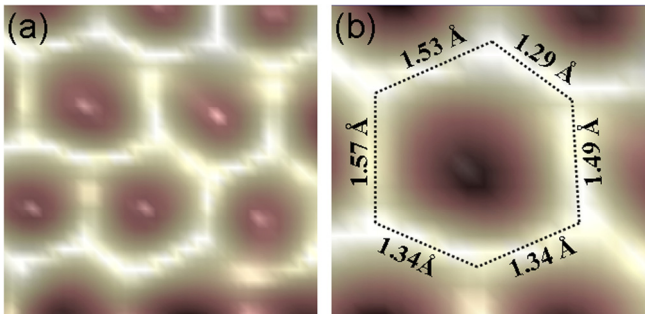


**Figure 5.** 6.9×6.9 Å$^2$ (a) and 4×4 Å$^2$ (b) STM images illustrating the distortion of the carbon-carbon bond lengths in the graphene monolayer on cubic-SiC(001). The lengths of all sides of the distorted hexagon overlaid on the STM image in (b) are indicated for clarity.

S1b). It is known that electronic edge states in graphene can induce additional modulations in STM images of graphene nanoribbons [28] and increase the periodicity of the atomically resolved patterns near the ribbon edges [29], which is also discernible in Figs. 2a and S1b. The asymmetry of the carbon-carbon bond lengths in the graphene monolayer on SiC(001) is illustrated in Fig. 5. The contrast in atomically resolved STM images was adjusted to enhance the bond length distribution in small domain regions, which can be considered as planar. The STM image in Fig. 5a demonstrates the irregular distortion of the graphene honeycomb lattice. For clarity a distorted hexagon is overlaid on the STM image in Fig. 5b. Although the apparent lengths of the carbon-carbon bonds in scanning probe microscopy images can be modified by tip-surface interaction [30], the values shown in Fig. 5b agree with the bond distribution calculated in Ref. [24] for a rippled graphene monolayer.

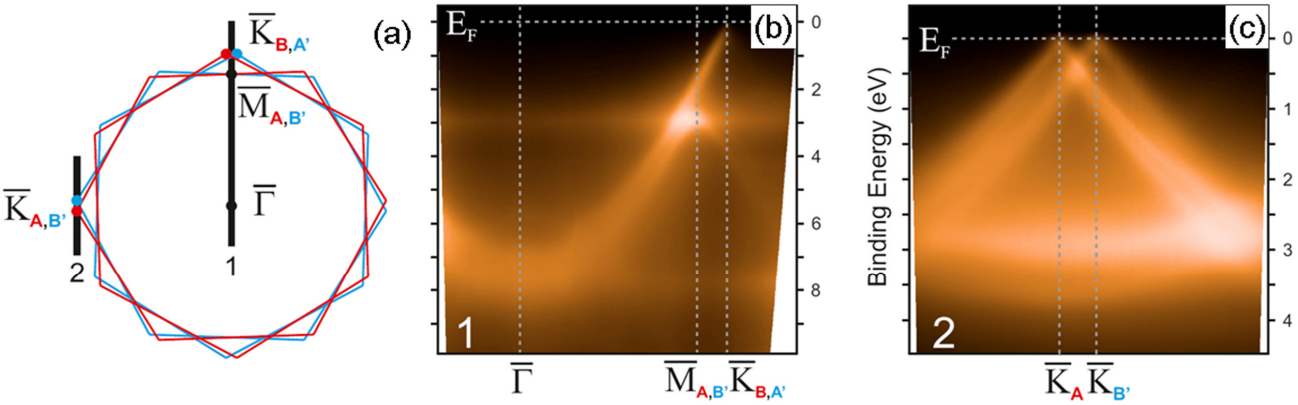


**Figure 6.** (a-c) ARPES characterization of graphene grown on cubic-SiC(001). (a) Effective surface Brillouin zone as seen in ARPES due to superposition of signals from the four domains. The four domains are marked by letters A, B, A', B' as in Fig. 4. (b,c) Dispersion of π--band in graphene measured by ARPES along directions 1 and 2 as denoted in (a).

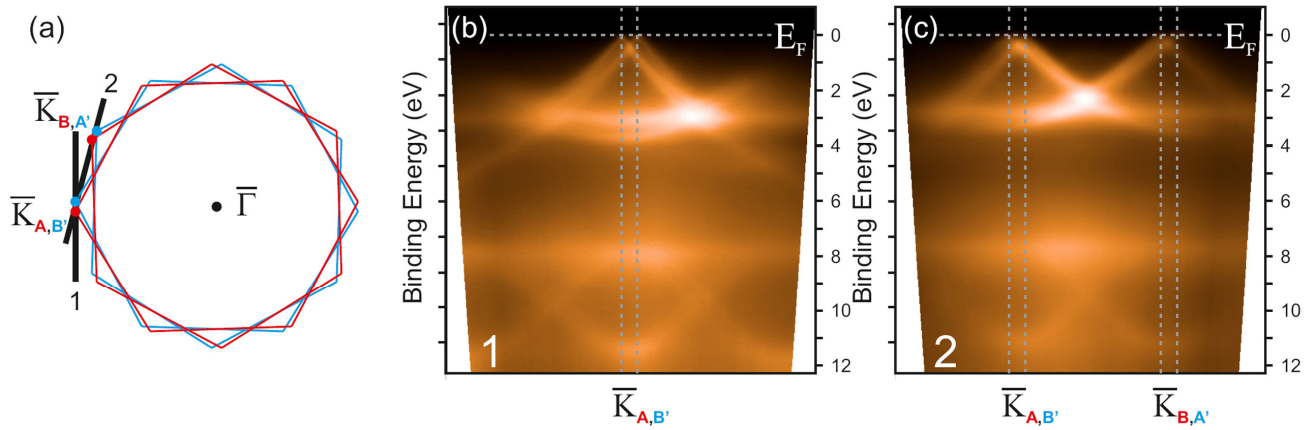


**Figure 7.** Angle-resolved photoemission from graphene/SiC(001). (a) Effective surface Brillouin zone corresponding to four rotated domain variants. (b, c) Dispersion of π-band in graphene along directions 1 and 2, correspondingly, as denoted in (a).

The quasi-freestanding character of graphene monolayers on SiC(001) is further confirmed by angle-resolved photoemission measurements of the π-band which are reported in Fig. 6 and 7. Since ARPES is a non-local probe method which sums up photoelectrons from a wide sample area, the effective surface Brillouin zone of graphene on SiC(001) comprises Brillouin zones of all rotated domains, according to the sketch shown in Fig. 6a. Such an effective Brillouin zone can be directly derived from the superposition LEED pattern displayed in Fig. 1d.

The band structure of graphene/SiC sample measured along the $\overline{\Gamma}\overline{K}$-direction of the surface Brillouin zone (thick black line denoted by "1" in Fig.6a) reveals the characteristic dispersion of the π-band reaching the Fermi level. This is in contrast with the first publications on graphene/SiC(001) synthesis where a 0.25 eV shift of the Dirac point was reported [11]. The sharp and narrow character of a single graphene band clearly shows that trilayer graphene on SiC(001) possesses the electronic properties of monolayer graphene. Fig. 6b also displays a dispersion of the π-band which backfolds at ~2.5 eV binding energy and originates from the $\overline{M}$-point of the rotated graphene domain.

In order to determine the energy of the Dirac point and to find out the charge doping of graphene

in our samples, we went to detection geometry perpendicular to $\bar{\Gamma}\bar{K}$-direction where the interference of photoelectrons on graphene sublattices is suppressed and both sides of the Dirac cone are observed in photoemission [31]. The resulting ARPES data are shown in Fig. 6c. The corresponding measurement position in the effective Brillouin zone is shown by a thick black line denoted with "2" in Fig. 6a. In Fig. 7, two more spectra are shown. One sees that the Dirac cones sampled from all rotated domains look identical, and their Dirac crossing points are very close to the Fermi level. The similarity of the electronic structure of the rotated domains, the charge neutrality and the absence of any apparent hybridization effects with SiC, indicate that graphene possesses the electronic properties of a freestanding monolayer. Note that the same pattern of 24 Dirac points coming to the Fermi level was observed at all areas of the studied samples.

The observed structure is fully consistent with the co-existence of AA' and BB' domains and independently confirms that all 24 diffraction spots observed in LEED experiments (as well as all 24 Dirac points seen in ARPES) originate from the single graphene monolayer, and not from rotated layers in a bilayer structure. Nevertheless, we have to remark that the ARPES dispersion shown in Fig. 6c reveals tiny additional bands seen between the two split Dirac cones. These bands might be traces of a graphene bilayer and suggest small imperfections present in particular samples. The bilayer dispersion curves shifted from the Fermi level are better seen in the differentiated spectra shown in Fig. S4b and S4c. However, the minor contribution from bilayer regions proves the very weak interaction of individual layers within the trilayer graphene on cubic-SiC(001). Multilayer graphite-like structures covering the SiC substrate are not supported by the presented ARPES data that simultaneously reveal sharp linear dispersions crossing the Fermi level and very weak bilayer contributions.

In summary, we have demonstrated that continuous and uniform trilayer graphene can be synthesized on thin cubic-SiC(001)/Si(001) wafers. LEEM, STM and ARPES studies prove very weak interaction of individual layers with one another and with the SiC substrate. Therefore, the synthesized graphene trilayers possess the physical properties of monolayer graphene and can be more inert than a single graphene monolayer, giving additional perspectives for synthesis and technological applications. The presented data support the view that graphene grown on SiC(001) films deposited on standard Si(001) wafers can be the next decisive step towards graphene-based electronics.

## Acknowledgements

This work supported by the Russian Academy of Sciences, RFBR grants № 11-02-01253 and 11-02-01256, by Marie Curie IIF grant within the 7th European Community Framework Programme and by SPP 1459 of the Deutsche Forschungsgemeinschaft. We thank T. Chassagne, M. Zielinski and M. Portail (CRHEA-CNRS, Sophia Antipolice, France) for providing SiC samples and S. I. Bozhko and V. N. Semenov for help with the preparation of single crystalline tungsten probes.

## Electronic Supplementary Material:

Supplementary material is available in the online version of this article at http://dx.doi.org/***

## References

[1] Novoselov, K. S.; Geim, A. K.; Morozov, S. V.; Jiang, D.; Zhang, Y.; Dubonos, S. V.; Grigorieva, I. V.; Firsov, A. A. Electric field effect in atomically thin carbon films. *Science* **2004**, 306, 666-669.

[2] Novoselov, K. S.; Geim, A. K.; Morozov, S. V.; Jiang, D.; Katsnelson, M. I.; Grigorieva, I. V.; Dubonos, S. V.; Firsov, A. A. Two-dimensional gas of massless Dirac fermions in graphene. *Nature* **2005**, 438, 197-200.

[3] Sprinkle, M.; Siegel, D.; Hu, Y.; Hicks, J.; Tejeda, A.;

Taleb-Ibrahimi, A.; Le Fevre, P.; Bertran, F.; Vizzini, S.; Enriquez, H.; Chiang, S.; Soukiassian, P.; Berger, C.; de Heer, W. A.; Lanzara, A.; Conrad, E. H. First direct observation of a nearly ideal graphene band structure. *Phys. Rev. Lett.* **2009**, 103**,** 226803.

[4] Berger, C.; Song Zhimin; Li Tianbo; Li Xuebin; Ogbazghi, A. Y.; Feng Rui; Dai Zhenting; Marchenkov, A. N.; Conrad, Ed. H.; First, Ph. N.; de Heer, W. A. Ultrathin Epitaxial Graphite: 2D Electron Gas Properties and a Route toward Graphene-based Nanoelectronics. *J. Phys. Chem. B* **2004**, 108, 19912-19916.

[5] Berger, C.; Song Zhimin; Li Xuebin; Wu Xiaosong; Brown, N.; Naud, C.; Mayou, D.; Li, T.; Hass, J.; Marchenkov, A. N.; Conrad, Ed. H.; First, Ph. N.; de Heer, W. A. Electronic Confinement and Coherence in Patterned Epitaxial Graphene. *Science* **2006**, 312, 1191-1196.

[6] Emtsev, K.V.; Bostwick, A.; Horn, K.; Jobst, J.; Kellogg, G. L.; Ley, L.; McChesney, J.; Ohta, T.; Reshanov, S. A.; Rohr, J.; Rotenberg, E.; Schmid, A. K.; Waldmann, D.; Weber, H. B.; Seyller, T. Towards wafer-size graphene layers by atmospheric pressure graphitization of silicon carbide. *Nat. Mater.* **2009**, 8**,** 203-207.

[7] Ouerghi, A.;; Kahouli, A.; Lucot, D.; Portail, M.; Travers, L.; Gierak, J.; Penuelas, J.; Jegou, P.; Shukla, A.; Chassagne, T.; Zielinski, M. Epitaxial graphene on cubic SiC(111)/Si(111) substrate. *Appl. Phys. Lett.* **2010**, 96, 191910.

[8] Coletti, C.; Emtsev, K. V.; Zakharov, A. A.; Ouisse, T.; Chaussende, D.; Starke, U. Large area quasi-free standing monolayer graphene on 3C-SiC(111). *Appl. Phys. Lett.* **2011**, 99, 081904.

[9] Portail, M.; Michon, A.; Vezian, S.; Lefebvre, D.; Chenot, S.; Roudon, E.; Zielinski, M.; Chassagne, T.; Tiberj, A.; Camassel, J.; Cordier, Y. Growth mode and electric properties of graphene and graphitic phase grown by argon-propane assisted CVD on 3C-SiC/Si and 6H-SiC. *Journal of Crystal Growth* **2012**, 349, 27-35.

[10] Suemitsu, M.; Fukidome, H. Epitaxial graphene on silicon substrates. *J. Phys. D: Appl. Phys.* **2010**, 43, 374012.

[11] Aristov, V. Yu.; Urbanik, G.; Kummer, K.; Vyalikh, D. V.; Molodtsova, O. V.; Preobrajenski, A. B.; Zakharov, A. A.; Hess, Ch.; Hänke, T.; Büchner, B.; Vobornik, I.; Fujii, J.; Panaccione, G.; Ossipyan, Yu. A.; Knupfer, M. Graphene synthesis on cubic SiC/Si wafers. Perspectives for mass production of graphene-based electronic devices. *Nano Letters* **2010**, 10, 992-995.

[12] Ouerghi, A.; Ridene, M.; Balan, A.; Belkhou, R.; Barbier, A.; Gogneau, N.; Portail, M.; Michon, A.; Latil, S.; Jegou, P.; Shukla, A. Sharp interface in epitaxial graphene layers on 3*C*-SiC(100)/Si(100) wafers. *Phys. Rev. B* **2011**, 83, 205429.

[13] Hass, J.; Varchon, F.; Millan-Otoya, J. E.; Sprinkle, M.; Sharma, N.; de Heer, W. A.; Berger, C.; First, P. N.; Magaud, L.; Conrad, E. H. Why multilayer graphene on 4H-SiC(0001) behaves like a single sheet of graphene. *Phys. Rev. Lett*. **2008**, 100, 125504.

[14] Semond, F.; Soukiassian, P.; Mayne, A.; Dujardin, G.; Douillard, L.; Jaussaud, C. Atomic Structure of the β-SiC(100)-(3×2) Surface. *Phys. Rev. Lett.* **1997**, 77, 2013-2016.

[15] Soukiassian, P.; Semond, F.; Douillard, L.; Mayne, A.; Dujardin, G.; Pizzagalli, L.; Joachim, C. Direct Observation of a β-SiC(100)-*c*(4×2) Surface Reconstruction. *Phys. Rev. Lett.* **1997**, 78, 907-910.

[16] Aristov, V. Yu.; Douillard, L.; Fauchoux, O.; Soukiassian, P. Temperature-Induced Semiconducting *c*(4×2) ↔ Metallic (2×1) Reversible Phase Transition on the β-SiC(100) Surface. *Phys. Rev. Lett.* **1997**, 79, 3700-3703.

[17] Derycke, V.; Soukiassian, P.; Mayne, A.; Dujardin, G. Scanning tunneling microscopy investigation of the C-terminated β-SiC(100) c(2×2) surface reconstruction: dimer orientation, defects and antiphase boundaries, *Surf. Sci.* **2000**, 446, L101–L107.

[18] Doillard, L.; Aristov, V. Yu.; Semond, F.; Soukiassian, P. Pairs of Si atomic lines self-assembling on the b-SiC(001) surface: an 8×2 reconstruction. *Surf. Sci.* **1998**, 401, L395-L401.

[19] Hupalo, M.; Conrad, E. H.; Tringides, M. C. Growth mechanism for epitaxial graphene on vicinal 6*H*-SiC(0001) surfaces: A scanning tunneling microscopy study. *Phys. Rev. B* **2009**, 80, 041401(R).

[20] Hass, J.; de Heer, W. A.; Conrad, E. H. The growth and morphology of epitaxial multilayer graphene. *J. Phys. Condens. Matter.* **2008**, 20, 323202.

[21] Hibino, H.; Kageshima, H.; Maeda, F.; Nagase, M.; Kobayashi, Y.; Yamaguchi, H. Microscopic thickness determination of thin graphite films formed on SiC from quantized oscillation in reflectivity of low-energy electrons. *Phys. Rev. B* **2008**, 77, 075413.

[22] Riedl, C.; Coletti, C.; Iwasaki, T.; Zakharov, A. A.; Starke, U. Quasi-Free-Standing Epitaxial Graphene on SiC Obtained by Hydrogen Intercalation. *Phys. Rev. Lett.* **2009**, 103, 246804.

[23] Meyer, J.C.; Geim, A.K.; Katsnelson, M. I.; Novoselov, K.S.; Booth, T.J.; Roth, S. The structure of suspended graphene sheets. *Nature* **2007**, 446, 60-63.

[24] Fasolino, A.; Los, J. H; Katsnelson, M. I. Intrinsic ripples in graphene. *Nature Mater.* **2007**, 6, 858-861.

[25] Mashoff, T.; Pratzer, M.; Geringer, V.; Echtermeyer, T. J.; Lemme, M. C.; Liebmann, M.; Morgenstern, M. Bistability and Oscillatory Motion of Natural Nanomembranes Appearing within Monolayer Graphene on Silicon Dioxide. *Nano Letters* **2010**, 10, 461-465.

[26] Horcas, I.; Fernandez, R.; Gomez-Rodriguez, J.M.; Colchero, J.; Gomez-Herrero, J.; Baro, A.M. WSxM: A software for scanning probe microscopy and a tool for nanotechnology. *Rev. Sci. Instrum.* **2007**, 78, 013705.

[27] Huang, P. Y.; Ruiz-Vargas, C. S.; van der Zande, A. M.; Whitney, W. S.; Levendorf, M. P.; Kevek, J. W.; Garg, S.; Alden, J. S.; Hustedt, C. J.; Zhu, Y.; Park, J.; McEuen, P. L.; Muller, D. A. Grains and grain boundaries in single-layer graphene atomic patchwork quilts. *Nature* **2011**, 469, 389-392.

[28] Tao, C.; Jiao, L.; Yazyev, O. V.; Chen, Y.-C.; Feng, J.; Zhang, X.; Capaz, R. B.; Tour, J. M.; Zettl, A.; Louie, S. G.; Dai, H.; Crommie, M. F. Spatially resolving edge states of chiral graphene nanoribbons. *Nature Phys.* **2011**, 7, 616-620.

[29] Tapaszto, L.; Dobrik, G.; Lambin, P.; Biro, L. P. Tailoring the atomic structure of graphene nanoribbons by scanning tunnelling microscope lithography. *Nature Nanotechnology* **2008**, 3, 397-401.

[30] Gross, L.; Mohn, F.; Moll, N.; Schuler, B.; Criado, A.; Guitian, E.; Pena, D.; Gourdon, A.; Meyer, G. Bond-order discrimination by atomic force microscopy. *Science* **2012**, 337, 1326-1329.

[31] Shirley E. L; Terminello L. J.; Santoni A.; Himpsel F. J. Brillouin-zone-selection effects in graphite photoelectron angular distributions. *Phys. Rev. B* **1995**, 51, 13614-13622.

.

# Electronic Supplementary Material

# Continuous Wafer-Scale Graphene on cubic-SiC(001)

Alexander N. Chaika[1,2](✉), Olga V. Molodtsova[3], Alexei A. Zakharov[4], Dmitry Marchenko[5], Jaime Sánchez-Barriga[5], Andrei Varykhalov[5], Igor V. Shvets[2], Victor Yu. Aristov[1,3]

[1]Institute of Solid State Physics RAS, Chernogolovka, Moscow District 142432, Russia

[2]Centre for Research on Adaptive Nanostructures and Nanodevices (CRANN), School of Physics, Trinity College, Dublin 2, Ireland

[3]HASYLAB at DESY, D-22607 Hamburg, Germany

[4]MAX-lab, Lund University, Box 118, 22100 Lund, Sweden

[5]Helmholtz-Zentrum Berlin für Materialien und Energie, D-12489 Berlin, Germany

Supporting information to DOI 10.1007/s12274-****-****-* (automatically inserted by the publisher)

Uniform graphene layers were fabricated on commercially available cubic-SiC(001) films on on-axis Si(001) wafers using Si-atom sublimation followed by SiC surface layer graphitization during high-temperature annealing in controlled ultrahigh vacuum (UHV) conditions according to the procedure described in [S1]. At the first stage of graphene preparation, several monolayers of Si atoms were deposited onto a pre-annealed carbon-rich SiC(001)1×1 surface. Then, the SiC surface was annealed at gradually increasing temperatures in the 800–1300ºC range giving rise to Si atom sublimation. According to our low-energy electron diffraction (LEED) and atomically resolved scanning tunnelling microscopy (STM) data, Si-rich 3×2 and 5×2, Si-terminated stoichiometric c(4×2) and C-terminated stoichiometric SiC(001)-c(2×2) reconstructions [S2] were successively fabricated. Finally, to convert the carbon–carbon bonds of the c(2×2) surface structure into $sp^2$graphene bonds, flash heatings at elevated temperatures (1300–1350°C) were applied.

The graphene synthesis on the SiC(001) surface and extensive in-situ STM studies of its atomic structure were carried out in the UHV chamber of an LAS-3000 (RIBER) electron spectrometer equipped with a room-temperature STM GPI-300. The base pressure in the spectrometer

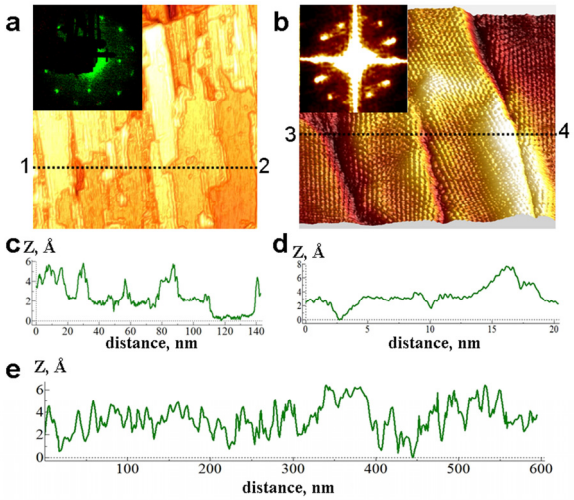


**Figure S1.** (a): Large-area STM image of graphene on SiC(001) and LEED pattern (inset at the top left corner, $E_p$=65 eV) measured from the same sample. (b): Atomically resolved STM image demonstrating several rotated domains and boundaries between individual graphene nanoribbons. Inset shows the 2D fast Fourier transform of the image. (c, d): Cross sections 1–2 (c) and 3–4 (d) of the images in Panels a and b, respectively. (e): Cross section of a large-area STM image (not shown here) demonstrating a peak-to-peak height difference below 1 nm on a micrometre scale surface region. The cross sections, quasi-3D views of the STM images and FFT pattern were prepared using WSXM software [S5].

Address correspondence to chaika@issp.ac.ru (Alexander N. Chaika)

chamber was kept below $8\times10^{-11}$ mbar. The pressure did not exceed $1.5\times10^{-10}$ mbar and $8\times10^{-10}$ mbar during the SiC(001) surface preparation and high-temperature graphene synthesis, respectively. To obtain detailed information about the atomic structure of the graphene layer on the SiC(001) surface, around 250 large-area and 400 atomically resolved STM images of different surface regions were taken from several samples prepared using the same procedure. For STM experiments we used chemically etched tips fabricated from [001]- and [111]-oriented single crystalline bars.

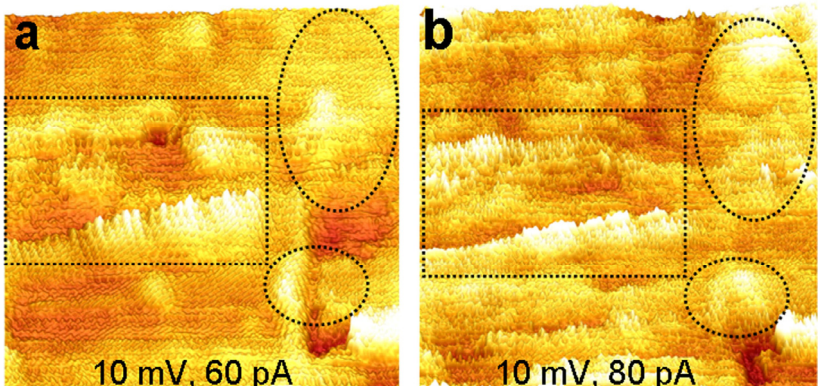


**Figure S2.** (a, b) Atomically resolved STM images of the same surface region of graphene/SiC(001) measured with the same tungsten tip at tunnelling parameters indicated on the panels. The images illustrate the flexibility of graphene layer suggesting it is decoupled from the substrate surface layer similar to that in exfoliated graphene [S4]. Minor variation of the tunnelling current leads to substantial change of the apparent layer morphology morphology because of tip–sample interaction.

As revealed by these STM studies, after the above-mentioned treatment, the SiC(001) surface was covered by rippled graphene domains with lateral dimensions ranging from several nm to 20–30 nm. A typical atomically resolved STM image of the graphene layer on cubic-SiC(001) is shown in Fig. S1b. According to the STM data, the individual domains are rippled (Fig. 2) in accordance with the theoretical predictions for the freestanding 2D graphene layer [S3]. The apparent layer roughness was found to be essentially dependent on the applied tunneling parameters (bias voltage and tip–sample distance). This is illustrated by Fig. S2, demonstrating a substantial change of the surface topography with increasing tunnelling current. This effect was reproducibly observed in a series of atomically resolved experiments. The dependence of the apparent surface roughness on the applied tunneling parameters qualitatively reproduced the effect of the motion of a graphene monolayer on a $SiO_2$ substrate induced by the tip–sample interaction [S5]. This proves the free-standing character of the graphene layers on SiC(001). High-resolution core level C 1*s* spectra taken from the investigated samples demonstrate only two narrow components (FWHM of graphene C 1*s* component was around 0.3 eV) with energies corresponding to bulk SiC and single-layer graphene, which prove the absence of a buffer layer.

The cross sections in Fig.S1c and S1d show that central parts of the graphene domains are elevated by several Ångströms (Å) relative to the valleys where the graphene sheets are most probably attached to the SiC substrate and other graphene domains. The observed morphology of the graphene layer is in agreement with the theoretical models for this 2D crystal [S3]. The rippling of the domains led to a root mean square roughness of the micrometer-scale STM images ranging from 2.5 to 3.0 Å. As illustrated by the cross section of a 600×600 $nm^2$ STM image presented in Fig. S1e, this corresponds to a peak-to-peak height difference of several Å along the micrometer-scale line scan. Despite the apparent roughness of the surface graphene layer, we did not observe any single- or double-layer height steps in our atomically resolved STM experiments. On the contrary, detailed analysis of the valleys in atomically resolved STM images typically revealed either a bent continuous graphene layer (Fig. S3a) or boundaries between non-rotated (Fig. S3b) or rotated (Fig. S3c) rippled graphene domains.

The micro-scale continuity of the graphene overlayer and its rippling, the strong dependence of the

apparent surface topography on the tip–sample distance, the flexibility of the top layer, and the high intensity of the SiC(001) substrate diffraction spots that can be clearly observed along with the 24 graphene spots (inset in Fig. S1a) prove the high quality and free-standing character of graphene layers synthesized on cubic-SiC(001) surfaces.

LEEM and PES experiments were carried out on the samples prepared and analyzed in the STM GPI-300 chamber. Before the measurements, well prepared graphene/SiC(001) samples were annealed in the UHV chambers at temperatures of 200-1000°C to remove possible contamination. ARPES experiments were performed with an ARPES 1² endstation equipped with a hemispherical electron analyser Scienta R8000. The ARPES endstation is operated at UE112-PGM2a beamline at BESSY-II. All ARPES measurements were performed at a photon energy of 62 eV with a linear (mixed *s*+*p*) polarization of the light. The size of the photon spot at the sample was about 0.4 mm, which means that the ARPES signal contained a superposition of the photoemission from all rotational variants (domains) of graphene on SiC samples. The LEEM measurements were done using a SPELEEM microscope (Elmitec GmbH) installed on beamline I311 at the MAX-laboratory in Sweden. High resolution micro-PES C1s core level spectra of the graphene/SiC(001) samples were measured in the "normal incidence - normal emission" geometry using the SPELEEM microscope at the MAX-laboratory in Sweden.

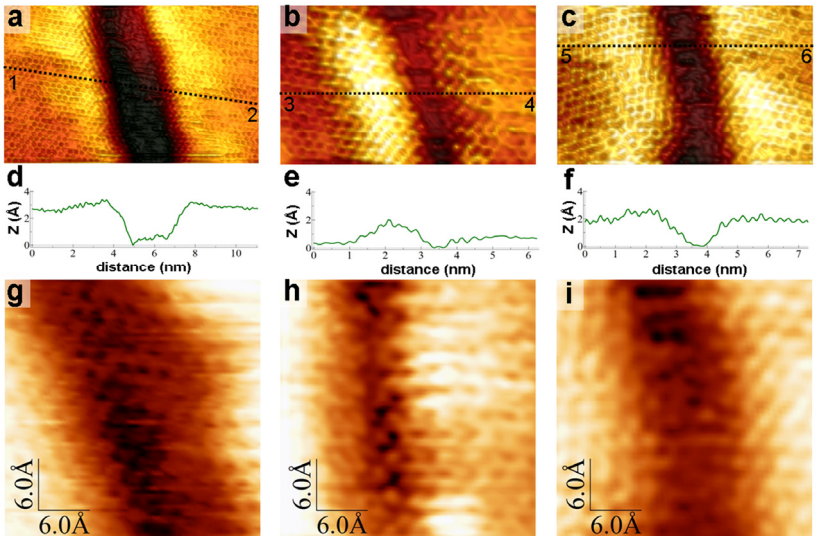


**Figure S3.** (a–c): STM images of different graphene nanoribbon (nanodomain) grain boundaries. (d–f): Cross sections 1–2 (d), 3–4 (e), and 5–6 (f) of the images in Panels a, b, and c, respectively. (g–i): Zoom (3×3 nm$^2$) regions of the graphene domain boundaries shown in Panels a–c, respectively.

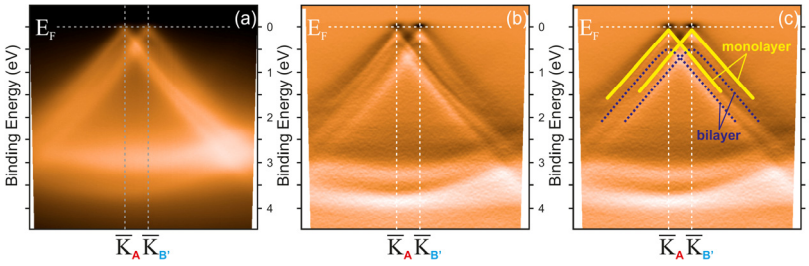


**Figure S4.** (a) Dispersion of the π-band in graphene on cubic-SiC(001)/Si(001) along direction 2 shown in Fig. 6a. (b,c) Derivative by energy of the dispersion at panel (a) proving the major contribution from the monolayer graphene and a minor contribution from bilayer graphene regions. Linear dispersions from two 27°-rotated monolayer graphene domains and weak shifted curves typical for bilayer graphene are schematically shown in panel (c).

**References of SM**


[S1] Aristov, V. Yu. et al. *Nano Letters* **2010**, *10*, 992.

[S2] Derycke, V. et al. *Phys. Rev. Lett.* **1998**, *81*, 5868.

[S3] Fasolino, A., Los, J. H., Katsnelson, M. I. *Nat. Mater.* **2007**, *6*, 858.

[S4] Mashoff, T. et al. *Nano Letters* **2010**, *10*, 461.

[S5] Horcas, I. et al. *Rev. Sci. Instrum*. **2007**, *78*, 013705.